

1 **Narrowband Clusteroluminescence with 100% Quantum Yield**
2 **Enabled by Through-Space Conjugation of Asymmetric**
3 **Conformation**

4
5 Yipu Wang,^{1,2,#} Jianyu Zhang,^{3,#} Weihao Tu,^{1,2,4} Lei Wang,^{1,2} Yuan Xie,^{1,2} Jing Zhi Sun,^{1,4} Feihe
6 Huang,^{2,5} Haoke Zhang,^{1,2,7,*} and Ben Zhong Tang^{1,3,6,*}

7 ¹MOE Key Laboratory of Macromolecular Synthesis and Functionalization, Department of
8 Polymer Science and Engineering, Zhejiang University, Hangzhou, 310058, China

9 ²Zhejiang-Israel Joint Laboratory of Self-Assembling Functional Materials, ZJU-Hangzhou
10 Global Scientific and Technological Innovation Center, Zhejiang University, Hangzhou 311215,
11 China

12 ³Department of Chemistry, Hong Kong Branch of Chinese National Engineering Research Center
13 for Tissue Restoration and Reconstruction, The Hong Kong University of Science and Technology,
14 Hong Kong, 999077, China

15 ⁴Centre of Healthcare Materials, Shaoxing Institute, Zhejiang University, Shaoxing 312000, China

16 ⁵Stoddart Institute of Molecular Science, Department of Chemistry, Zhejiang University,
17 Hangzhou, 310058, China

18 ⁶School of Science and Engineering, Shenzhen Institute of Aggregate Science and Technology,
19 The Chinese University of Hong Kong, Shenzhen (CUHK-SZ), Guangzhou 518172, China

20 [#]These authors contributed equally: Yipu Wang, Jianyu Zhang.

21 ^{*}Corresponding emails: zhanghaoke@zju.edu.cn (Haoke Zhang); tangbenz@cuhk.edu.cn (Ben Zhong
22 Tang)

23 **Abstract:** Different from traditional organic luminescent materials based on covalent
24 delocalization, clusteroluminescence (CL) from nonconjugated luminogens relies on noncovalent
25 through-space conjugation (TSC) of electrons. However, such spatial electron delocalization is
26 usually weak, resulting in low luminescent efficiency and broad emission peak due to multiple
27 vibrational energy levels. Herein, several nonconjugated luminogens are constructed by
28 employing biphenyl as the building unit to reveal the structure-property relationship and solve
29 current challenges. The intramolecular TSC could be gradually strengthened by introducing
30 building units and stabilized by rigid molecular skeleton and multiple intermolecular interactions.
31 Surprisingly, narrowband CL with full width at half-maximum of 40 nm and 100% efficiency is
32 successfully achieved via an asymmetric conformation, exhibiting comparable performance to the
33 traditional conjugated luminogens. This work realizes highly efficient and narrowband CL from
34 nonconjugated luminogens and highlights the essential role of structural conformation in
35 manipulating the photophysical properties of unconventional luminescent materials.

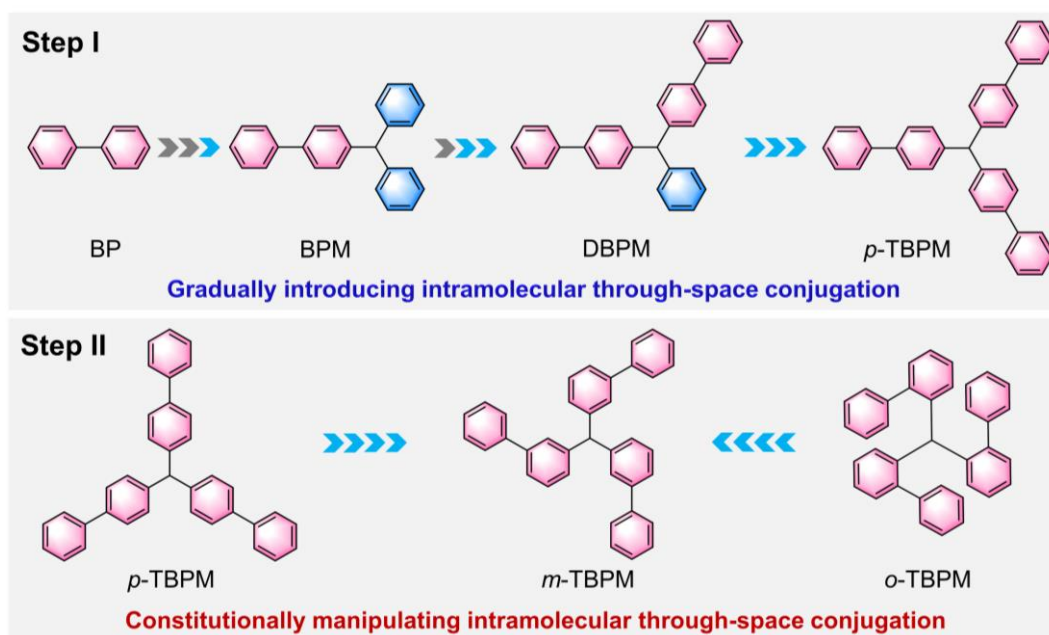
36 Introduction

37 The natural world follows a basic principle of modular assembly, where amino acids are
38 assembled into peptides and proteins and eventually into organisms.¹⁻³ Similarly, benzene rings
39 can be constructed into graphene and carbon nanotubes with unique functional properties.⁴⁻⁷ The
40 modular assembly usually endows materials with different properties and behaviors compared to
41 individual building units.⁸⁻¹⁰ Currently, the construction of organic luminescent materials is
42 typically achieved by covalently linking building units or incorporating donor-acceptor units,
43 where changes in their properties are primarily induced by electron delocalization or
44 charge-transfer effect.¹¹⁻¹⁷ However, in recent years, researchers have observed that specific
45 nonconjugated small molecules and polymers do not exhibit luminescence in solution but emit
46 intense light after forming clusters, known as clusteroluminescence (CL).¹⁸⁻²⁰ The working
47 mechanism of CL has been revealed to be through-space conjugation (TSC) of electrons between
48 isolated building units.^{21,22} Using common polyesters as an example, their building units (carbonyl
49 or ester) are connected through spatial *n-n* interactions, allowing the formation of TSC and the
50 generation of extrinsic long-wavelength fluorescence.²³⁻²⁵ Due to the poorly conjugated and
51 flexible structure, these materials possess excellent structural flexibility, processability,
52 biocompatibility, and degradability.²⁶⁻²⁹ These advantages show significant implications for
53 developing novel luminescent materials and hold particular value for practical applications.^{30,31}

54 Currently, the development of TSC-based emitters has gained considerable attention from
55 researchers.^{32,33} However, creating CL materials with exceptional performance that meet
56 application requirements remains a significant challenge.^{34,35} The production of CL relies on
57 noncovalent electron overlap and coupling of each unit, which requires the structural flexibility of
58 molecules to form close interactions of electrons in the excited state.^{36,37} Therefore, many reported
59 nonconjugated luminogens, such as triphenylmethane and tetraphenylethane, are constructed by
60 rigid building units, which rely on the flexibility of the molecular skeleton to form suitable
61 conformation for TSC.^{38,39} However, these luminescent materials based on TSC encounter several
62 issues, including unclear manipulation strategies due to vague structure-property relationship, low
63 luminescent efficiency due to structural flexibility and excited-state molecular motions, as well as
64 broad emission peaks with large full-width at half-maximum (FWHM) values due to numerous
65 vibrational energy levels.⁴⁰⁻⁴³ These challenges present significant obstacles to developing
66 efficient CL materials with high purity of emissive color.⁴⁴⁻⁴⁶ To address these challenges, one
67 approach is to transfer the flexibility from the molecular skeleton to the building units, forming
68 TSC via the flexibility of building units while maintaining the structural rigidity of the molecular
69 skeleton.⁴⁷⁻⁴⁹ By achieving strong TSC while minimizing vibrational motions upon
70 photoexcitation, it is possible to achieve narrowband CL with high luminescent efficiency.⁵⁰⁻⁵²

71 In this work, the simplest biphenyl (BP) is employed as the flexible building unit to construct
72 a series of nonconjugated luminogens, and the structure-property relationship of TSC and CL is

73 systematically studied via two molecule-engineering methods: gradually introducing building
 74 units and constitutionally adjusting the connecting positions of building units (**Fig. 1**). The former
 75 suggests the feasibility of using biphenyl as the building unit to enhance the strength of TSC, and
 76 the latter indicates the role of structural conformation in intra- and intermolecular interactions,
 77 which manipulate the stability of intramolecular TSC for CL. Interestingly, the first example of
 78 narrowband CL with an FWHM of 40 nm and 100% efficiency is successfully achieved via an
 79 asymmetric triarylmethane, which is comparable to the traditional conjugated narrowband
 80 luminogens. This work realizes the narrowband CL from nonconjugated luminogens with isolated
 81 biphenyls and provides a novel perspective to manipulate TSC for unconventional luminescent
 82 materials with high efficiency.



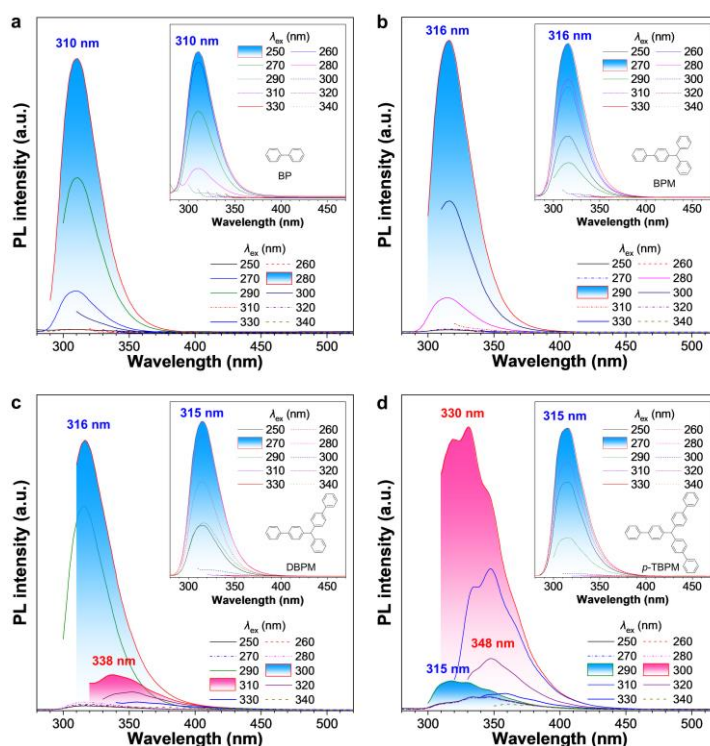
83
 84 **Fig. 1. The design strategy of nonconjugated molecules with narrowband clusteroluminescence**
 85 **using biphenyl as the building unit.**

86 Results

87 According to the above strategy, five compounds, 4-benzhydryl-1,1'-biphenyl (BPM),
 88 4,4''-(phenylmethylene)di-1,1'-biphenyl (DBPM), tri([1,1'-biphenyl]-4-yl)methane (*p*-TBPM),
 89 tri([1,1'-biphenyl]-3-yl)methane (*m*-TBPM), tri([1,1'-biphenyl]-2-yl)methane (*o*-TBPM) have
 90 been synthesized and fully characterized by using nuclear magnetic resonance spectra,
 91 high-resolution mass spectra, and high-performance liquid chromatography techniques
 92 (Supplementary **Figs. 1-32**). UV-visible absorption spectra of the building unit (e.g., BP) and the
 93 synthesized BPM, DBPM, and *p*-TBPM were performed in tetrahydrofuran (THF) solutions with
 94 different concentrations. The maximum absorption wavelength (λ_{abs}) of biphenyl is located at 249
 95 nm (Supplementary **Fig. 33**), suggesting its intrinsic through-bond conjugation. However, the λ_{abs}
 96 of BPM, DBPM, and *p*-TBPM are quite close to that of biphenyl (259 nm, 260 nm, and 263 nm,

97 respectively), indicating their nonconjugated structures. Meanwhile, the slight redshift is caused
98 by the hyperconjugation between the π units and the middle saturated carbon.

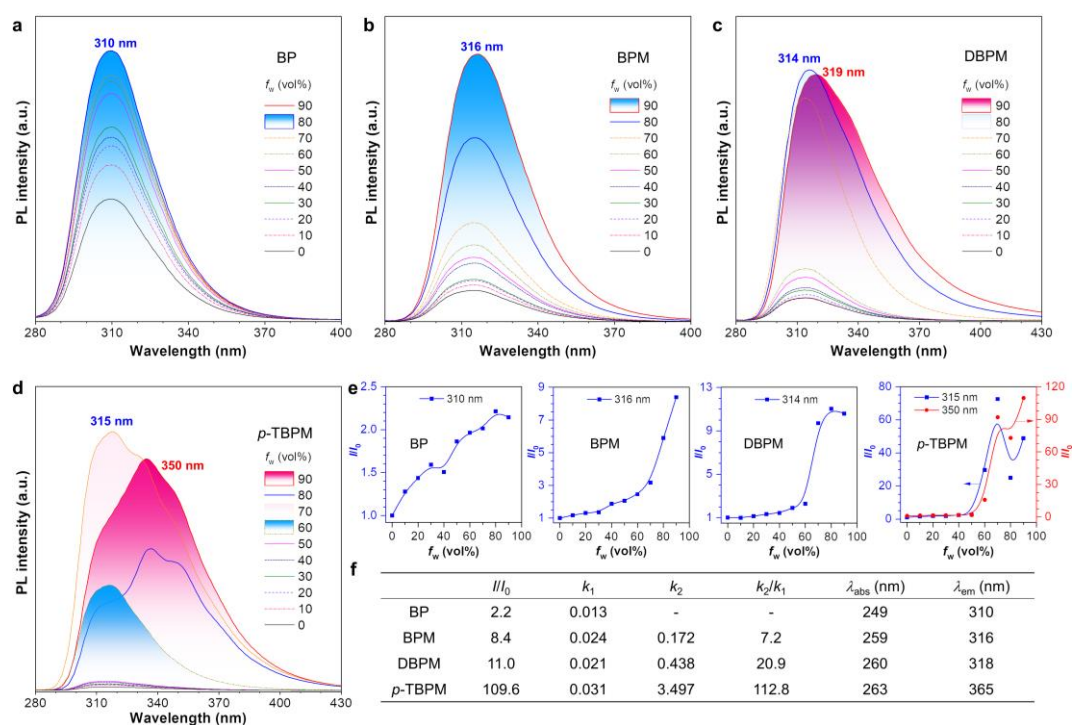
99 Then, the photoluminescence (PL) properties of these compounds were examined in THF
100 solution with different concentrations. **Fig. 2a** and Supplementary **Fig. 34a** demonstrate that BP
101 exhibits only one emission peak at 310 nm, and the position of the peak remains unchanged with
102 varying concentrations. Similar to BP, BPM displays only one intrinsic emission peak at 316 nm
103 in different concentrations, which is also attributed to the biphenyl unit (**Fig. 2b** and
104 Supplementary **Fig. 34b**). In contrast, DBPM exhibits a different behavior compared to the
105 previous two compounds. It shows only one intrinsic emission peak from the biphenyl unit with a
106 low concentration of 10^{-5} M, but a long-wavelength emission peak at 338 nm appears with a high
107 concentration of 10^{-3} M (**Fig. 2c** and Supplementary **Fig. 34c**). According to previous reports, it
108 should arise from the intramolecular TSC between two isolated biphenyl units of DBPM.
109 Compared to DBPM, *p*-TBPM already exhibits a distinct long-wavelength emission peak at 348 nm
110 nm in THF solution with a concentration of 10^{-4} M, which also excludes the possibility of
111 intermolecular interactions (Supplementary **Fig. 34d**). Moreover, the emission peak becomes
112 dominant when the concentration is increased to 10^{-3} M, indicating that *p*-TBPM has the strongest
113 intramolecular TSC among these four compounds (**Fig. 2d**).



114
115 **Fig. 2. Photophysical properties of BP, BPM, DBPM, and *p*-TBPM under different excitation**
116 **wavelengths. a** Photoluminescence (PL) spectra of BP, in THF solution (concentration = 10^{-3} M) under
117 different excitation wavelengths. **b** Photoluminescence (PL) spectra of BPM in THF solution
118 (concentration = 10^{-3} M) under different excitation wavelengths. **c** Photoluminescence (PL) spectra of
119 DBPM in THF solution (concentration = 10^{-3} M) under different excitation wavelengths. **d**
120 Photoluminescence (PL) spectra of *p*-TBPM in THF solution (concentration = 10^{-3} M) under different

121 excitation wavelengths. Inset: PL spectra of the corresponding compound in THF solution with a
 122 concentration of 10^{-5} M.

123 To investigate changes in CL behaviors of these compounds before and after aggregate
 124 formation, their PL spectra were further measured in THF/water mixtures with different water
 125 fractions (f_w) and the same concentration of 10^{-4} M. As expected, both BP and BPM only exhibit
 126 enhanced emission intensity with the increased f_w (Fig. 3a and 3b). Besides, the PL spectra of
 127 solid-state BP and BPM also show the intrinsic emission at 310 nm and 316 nm, respectively,
 128 indicating no formation of intramolecular TSC (Supplementary Fig. 35a and 35b). However, the
 129 photophysical behavior of DBPM in THF/water mixtures is different. When increasing f_w , its PL
 130 intensity continuously increased. When f_w reaches 90%, the emission peak redshifts from 315 nm
 131 to 319 nm with a vague shoulder peak (Fig. 3c). However, the solid-state PL spectra of DBPM do
 132 not exhibit a prominent long-wavelength emission peak (Supplementary Fig. 35c). These results
 133 indicate that the intramolecular TSC in DBPM is slightly enhanced but still weak. Significantly,
 134 the emission intensity of *p*-TBPM at 315 nm gradually increases when f_w increases from 0% to
 135 70%, but the shape of the emission peak changes, and a long-wavelength emission at 350 nm
 136 becomes distinct when f_w further increases to more than 80% (Fig. 3d). As a result, the PL
 137 intensity at $f_w = 90\%$ is 110 times higher than that in pure THF solution (Fig. 3e). The solid-state
 138 PL spectra of *p*-TBPM only shows the long-wavelength emission peak at 365 nm, suggesting the
 139 presence of the strongest intramolecular TSC among these four compounds (Supplementary Fig.
 140 35d).



141

142 **Fig. 3. Photophysical properties of BP, BPM, DBPM, and *p*-TBPM before and after aggregate**
 143 **formation. a** Photoluminescence (PL) spectra of BP in THF/water mixtures with different water

144 fractions (f_w), concentration (c) = 10^{-4} M. **b** Photoluminescence (PL) spectra of BPM in THF/water
145 mixtures with different water fractions (f_w), concentration (c) = 10^{-4} M. **c** Photoluminescence (PL)
146 spectra of DBPM in THF/water mixtures with different water fractions (f_w), concentration (c) = 10^{-4} M.
147 **d** Photoluminescence (PL) spectra of *p*-TBPM in THF/water mixtures with different water fractions
148 (f_w), concentration (c) = 10^{-4} M. **e** Plots of relative PL intensity (I/I_0) versus f_w of four compounds. I_0 =
149 intensity at f_w = 0%. **f** Summary of photophysical properties of four compounds. k_1 is the slope of I/I_0
150 with f_w from 0% to 60%; k_2 is the slope of I/I_0 with f_w from 60% to 90%; λ_{abs} is the maximum
151 absorption wavelength in THF solution; λ_{em} is the maximum emission wavelength in the solid state.

152 Subsequently, a semi-quantitative analysis was conducted to evaluate the influence of
153 aggregate formation by comparing the slopes of their relative PL intensity (I/I_0) in mixtures (**Fig.**
154 **3f**). k_1 and k_2 are defined as the slopes of PL intensity enhancement before and after the formation
155 of aggregates, respectively, and the ratio of k_2/k_1 represents the enhancement solely induced by
156 aggregation without the influence of the mixture polarity. It is found that the k_2/k_1 value gradually
157 increases along with the increased numbers of biphenyl units, from BPM of 7.2 to DBPM of 20.9
158 and *p*-TBPM of 112.8. This result further confirms that the intramolecular TSC could be stepwise
159 enhanced by introducing the flexible building unit of biphenyl, and *p*-TBPM shows the strongest
160 intramolecular TSC among these four compounds.

161 By gradually introducing biphenyl moieties, we have successfully constructed *p*-TBPM,
162 which exhibits highly efficient CL with an absolute quantum yield (Φ) of 55% (**Table 1**).
163 However, excitation-dependent emission in the solid state also indicates its flexible molecular
164 skeleton and formed TSC upon photoexcitation. Therefore, *m*-TBPM and *o*-TBPM were designed
165 and synthesized by changing the connecting position of three isolated biphenyl units to study the
166 constitutional manipulation of TSC and structural rigidity (**Fig. 1**). It was expected that altering
167 the position would adjust the distance and dihedral angle between every biphenyl, thereby
168 manipulating the intramolecular interaction of π electrons and TSC among biphenyl units.

169 The maximum absorption wavelengths of *m*-TBPM and *o*-TBPM in THF solution are located
170 at 255 nm and 230 nm, respectively, also indicating the nonconjugated nature of three biphenyl
171 moieties as *p*-TBPM. The PL properties of these two compounds were measured and compared
172 (Supplementary **Fig. 33**). In pure THF solution with a low concentration of 10^{-5} M, the
173 long-wavelength emission from TSC at 370 nm is already observable for *m*-TBPM, supporting its
174 intramolecular behaviors (**Fig. 4a** and **Supplementary Fig. 36a**). Besides, it completely
175 dominates when the concentration reaches 10^{-3} M and becomes excitation-independent, indicating
176 its strong and stable TSC. In THF/water mixtures, the emission originating from TSC displays
177 negligible change when f_w is less than 60%. As the $f_w \geq 70\%$, the long-wavelength emission from
178 TSC becomes detectable and gradually enhances, reaching an astonishing 136.5 times higher
179 when $f_w = 90\%$ than that in pure THF solution (**Fig. 4b**). Moreover, the solid-state PL spectra of
180 *m*-TBPM reveal an almost dominant and excitation-independent emission at 374 nm. Surprisingly,
181 the absolute Φ of solid *m*-TBPM reaches 100%, accompanied by a quite narrow peak with the

182 FWHM value of 40 nm, which is attributed to its stable and strengthened TSC with few
 183 vibrational energy levels (**Fig. 4c** and **Table 1**). To our knowledge, it is the first time for
 184 nonconjugated compounds to produce CL with such a high Φ , and the FWHM is comparable to
 185 the conventionally conjugated luminescent materials with narrowband emission.⁵³⁻⁵⁵ Therefore,
 186 *m*-TBPM should be a novel narrowband luminescent material based on the emerging TSC and CL.

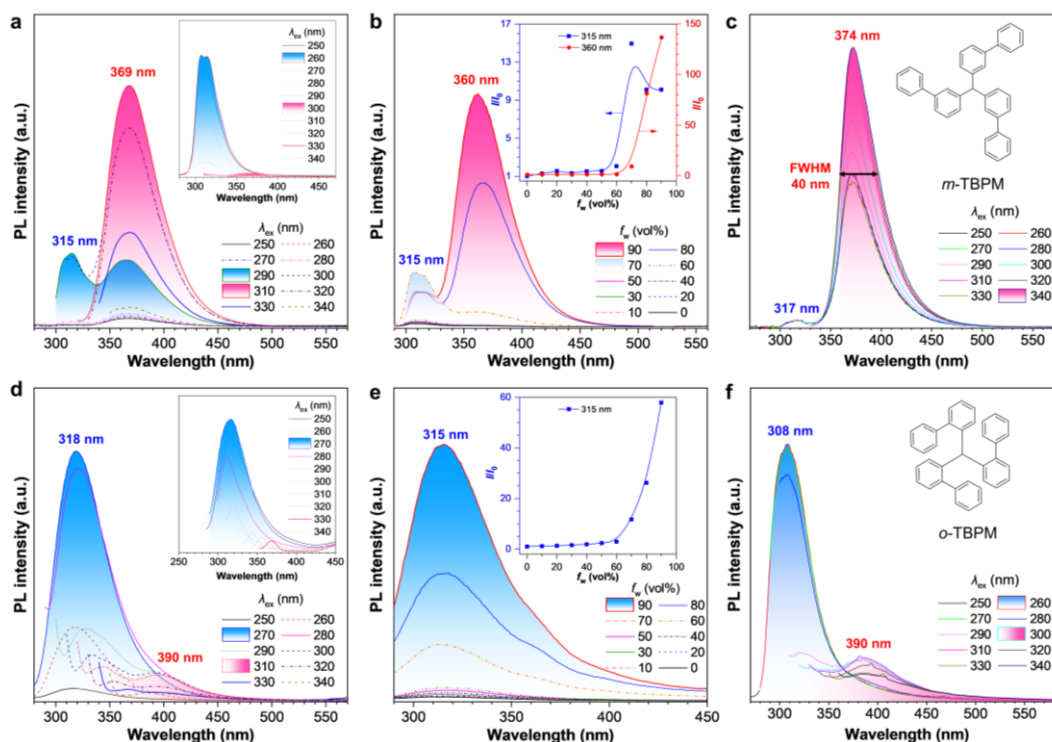
187 Based on the aforementioned design, it was expected that *o*-TBPM would exhibit the
 188 strongest intramolecular TSC due to the crowded molecular configuration that may help result in
 189 spatial electron delocalization. However, PL results show that only the intrinsic emission from
 190 TBC-based biphenyl units is detected at 318 nm in the dilute THF solution of 10⁻⁵ M, even in the
 191 THF/water mixtures with a *f_w* of 90% (**Fig. 4d** and **4e**). With the concentration of 10⁻³ M or in the
 192 solid state, a weak long-wavelength emission from TSC at 390 nm is observed, while the emission
 193 from TBC remains dominant throughout (**Fig. 4f**). In addition, the quantum yield of solid *o*-TBPM
 194 is only 4%, and the FWHM of the long-wavelength emission peak is extremely wide, exceeding
 195 70 nm (**Table 1**). It could be seen that adjusting the substituents to the *ortho*-position can indeed
 196 increase the overlap of delocalized electrons between the isolated units, as evidenced by the
 197 extended emission wavelength compared to the other two isomers. However, the crowded
 198 conformation also induces steric hindrance between biphenyls, resulting in dynamic molecular
 199 motions and an unstable TSC in the excited state. As a result, *o*-TBPM exhibits the longest
 200 emission wavelength of TSC at 390 nm but quite low emission efficiency compared to the other
 201 two isomers.

202 **Table 1. Photophysical properties of *p*-TBPM, *m*-TBPM, and *o*-TBPM^a**

	λ_{abs} (nm)	TBC emission		TSC emission			Φ (%)
		λ_{TBC} (nm)	τ (ns)	λ_{TSC} (nm)	FWHM (nm)	τ (ns)	
<i>p</i> -TBPM	263	-	-	365	53	2.76	55
<i>m</i> -TBPM	255	317	4.57	374	40	3.36	100
<i>o</i> -TBPM	230	308	1.49	390	>70	4.43	4

203 ^aAbbreviation: λ_{abs} = maximum absorption wavelength in the THF solution, TBC = through-bond
 204 conjugation, TSC = through-space conjugation, λ_{TBC} = maximum emission wavelength of TBC in the
 205 solid state, λ_{TSC} = maximum emission wavelength of TSC in the solid state, FWHM = full-width at
 206 half-maximum, τ = fluorescence lifetime, Φ = absolute quantum yield in the solid state.

207



208

209

Fig. 4. Photophysical properties of *m*-TBPM and *o*-TBPM. **a** Photoluminescence (PL) spectra of *m*-TBPM in THF solution under different excitation wavelengths, concentration (c) = 10^{-3} M. Inset: PL spectra of the corresponding compound in THF solution with a c of 10^{-5} M. **b** PL spectra of *m*-TBPM in THF/water mixtures with different water fractions (f_w), $c = 10^{-4}$ M. Inset: Plots of relative PL intensity (I/I_0) versus f_w . I_0 = intensity at $f_w = 0\%$. k_1 is the slope of I/I_0 with f_w from 0% to 60%; k_2 is the slope of I/I_0 with f_w from 60% to 90%. **c** PL spectra of solid-state *m*-TBPM under different excitation wavelengths. **d** Photoluminescence (PL) spectra of *o*-TBPM in THF solution under different excitation wavelengths, concentration (c) = 10^{-3} M. Inset: PL spectra of the corresponding compound in THF solution with a c of 10^{-5} M. **e** PL spectra of *o*-TBPM in THF/water mixtures with different water fractions (f_w), $c = 10^{-4}$ M. Inset: Plots of relative PL intensity (I/I_0) versus f_w . I_0 = intensity at $f_w = 0\%$. k_1 is the slope of I/I_0 with f_w from 0% to 60%; k_2 is the slope of I/I_0 with f_w from 60% to 90%. **f** PL spectra of solid-state *o*-TBPM under different excitation wavelengths.

211

212

213

214

215

216

217

218

219

220

221

222

223

224

225

226

227

228

229

230

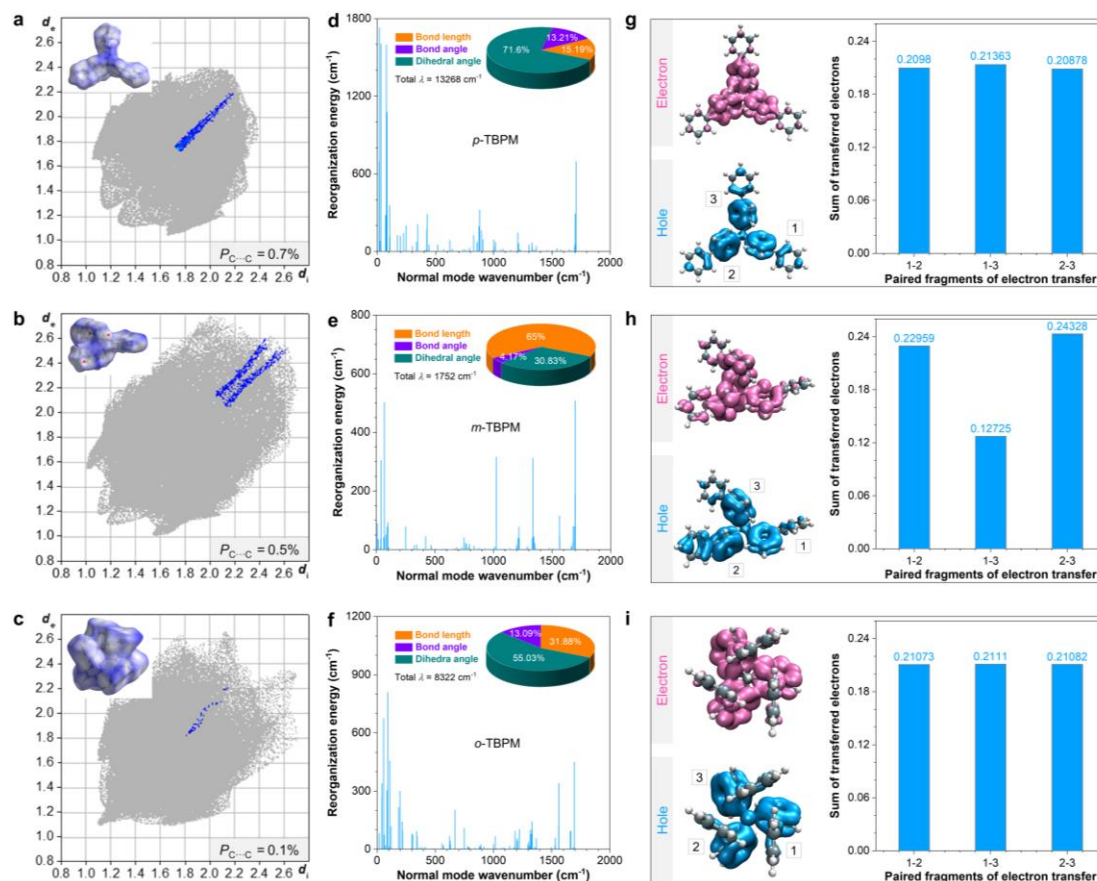
231

To explore the working mechanism and the difference in the photophysical properties among the three isomers of TBPM, Hirshfeld surface analysis, which is a quantitative analysis of intermolecular interactions based on single-crystal structures, was utilized.⁵⁶ As shown in **Fig. 5a-c**, intermolecular C-C interactions (blue shadows underneath the decomposed plot), which usually result in intermolecular interactions (e.g., π - π stacking) and long-wavelength emission from dimers, account for a negligible proportion of all intermolecular interactions (0.7%, 0.5%, and 0.1% for *p*-TBPM, *m*-TBPM, and *o*-TBPM, respectively). Thus, the results indicate that there is no obvious strong intermolecular interaction and clearly support the idea that the TSC and CL from these isomers are intramolecular behaviors. In addition, the proportions of weak C-H interactions of *p*-TBPM and *m*-TBPM are 48.6% and 46.5%, respectively, while the proportion of

232 *o*-TBPM is only 27.0% (Supplementary **Figs. 54-56**), which suggests that *o*-TBPM processes the
233 weakest intermolecular interactions to stabilize its geometry, which is consistent with its dynamic
234 rotations of biphenyl units.

235 Reorganization energy (λ) was analyzed to quantitatively evaluate their intrinsic geometric
236 changes under photoexcitation and the contributions of different intramolecular motions to
237 nonradiative decay (**Fig. 5d-f**).^{57,58} Among the three isomers, the total λ of *p*-TBPM is the largest
238 (13268 cm⁻¹), of which 71.60% is contributed by torsional motions of dihedral angles. Therefore,
239 *p*-TBPM processes significant geometric changes that dissipate energy through nonradiative decay
240 in the excited state. Similarly, the total λ of *o*-TBPM is 8322 cm⁻¹, and the contribution from
241 torsional motions of dihedral angles accounts for 55.03%. This result indicates its weak
242 intramolecular interactions due to the twisted structural conformation and steric hindrance of
243 biphenyl units. Thereby, both the weak intermolecular and intramolecular interactions destroy the
244 formed TSC and endow *o*-TBPM with the smallest Φ of CL in the solid state. Unexpectedly, the
245 total λ of *m*-TBPM is only 1752 cm⁻¹, and the contribution from motions of dihedral angles
246 declines to 30.83%, suggesting its rigid structural conformation and minimized vibrational energy
247 levels. Accordingly, it is believed that the TSC of *m*-TBPM could be stabilized by the stable
248 conformation in both solution and solid states, which endows it to emit strong CL in
249 low-concentration solutions as an isolated luminogen and narrowband CL in the solid state with
250 high purity of color and excitation-independent features (**Fig. 4a-f**).

251 For nonconjugated luminogens with CL properties, spatial electron overlap is a typical
252 characteristic. Therefore, hole-electron analysis was applied to study their electronic structure and
253 behaviors in the excited state (**Fig. 5g-i**). For these three compounds, the hole distribution is
254 located at three isolated biphenyl units. However, electron distribution forms noncovalent
255 delocalization around the central methyl group, forming the typical TSC of electrons that
256 promotes the long-wavelength CL. To provide a quantitative perspective, electron transitions and
257 redistributions from three nonconjugated biphenyl fragments were segmented and compared.
258 Interestingly, *p*-TBPM and *o*-TBPM exhibit electronic behaviors that are different from *m*-TBPM.
259 Three fragments of *p*-TBPM and *o*-TBPM contribute equally to the hole and electron. In contrast,
260 fragment 2 of *m*-TBPM dominates the hole and electron parts with contributions of 46.90% and
261 46.82%, respectively, while fragments 1 and 3 show smaller and relatively equal contributions
262 (Supplementary **Fig. S57a-c**). Similarly, the analysis of transferred electrons reveals that the
263 charge delocalization capability among the three fragments of *p*-TBPM and *o*-TBPM is equal,
264 while fragment 2 of *m*-TBPM exhibits a higher charge delocalization capability (**Fig. 5g-i and**
265 **Supplementary Fig. 57d-f**). These results indicate that the structural conformation and formed
266 TSC of *m*-TBPM are asymmetric, which should be also responsible for its highly efficient and
267 narrowband CL.

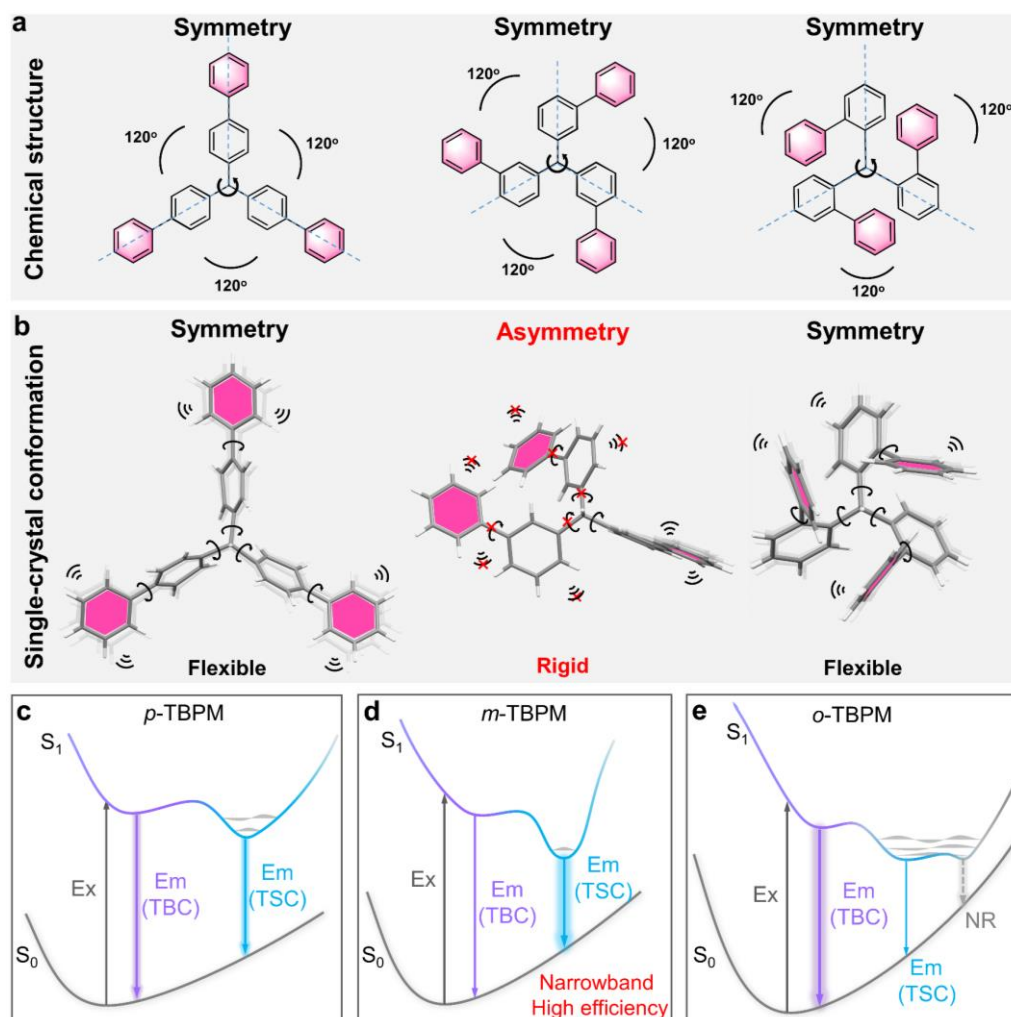


268

269 **Fig. 5. Theoretical calculations of *p*-TBPM, *m*-TBPM, and *o*-TBPM.** a-c Hirshfeld surfaces
 270 (mapped over d_{norm}) and decomposed fingerprint plots of intermolecular C-C interaction of (a) *p*-TBPM,
 271 (b) *m*-TBPM, and (c) *o*-TBPM. The full fingerprints appeared as grey shadows underneath decomposed
 272 plots, and intermolecular C...C interaction was shown as the blue shadow. $P_{C\cdots C}$ = proportion of
 273 intermolecular C...C interactions to total intermolecular interactions. d-e Plots of reorganization energy
 274 vs normal mode wavenumber of (d) *p*-TBPM, (e) *m*-TBPM, and (f) *o*-TBPM. g-i Hole-electron
 275 analysis and transferred electrons of paired fragments of (g) *p*-TBPM, (h) *m*-TBPM, and (i) *o*-TBPM.
 276

277 Based on the above analysis, we have gained insights into the molecular interactions,
 278 excited-state molecular motions, and electronic structure that influence the CL of these three
 279 isomers. To support the relationship between structural conformation and CL of these
 280 nonconjugated compounds, we further revisited their single-crystal structures and packing modes
 281 (Supplementary Figs. 58-60). Although the three compounds exhibit symmetric chemical
 282 structures with a C3 symmetry axis (Fig. 6a), their structural conformations of single molecules in
 283 the crystalline state differ significantly. Similar to their chemical structures, the structural
 284 conformations of *p*-TBPM and *o*-TBPM are close to symmetric. In contrast, the structural
 285 conformation of crystalline *m*-TBPM is asymmetric (Fig. 6b). Within the packing mode of
 286 *p*-TBPM, although there are many intermolecular interactions that could restrict intramolecular
 287 motions (Supplementary Fig. 58), its flexible skeleton cannot sufficiently stabilize the formed

288 TSC, endowing it with moderate Φ and FWHM of CL in the crystalline state. For *o*-TBPM,
 289 accompanied by the flexible biphenyl groups with steric hindrance, the limited number of
 290 intermolecular interactions cause dynamic molecular motions and energy dissipation, resulting in
 291 its lowest Φ of CL (Supplementary Fig. 59). On the other hand, the rigid molecular skeleton and
 292 numerous intermolecular interactions of *m*-TBPM block active intramolecular motions and
 293 facilitate the formation of stable TSC for highly efficient CL (Supplementary Fig. 60). Notably,
 294 no strong intermolecular interactions of π - π stacking for these three compounds are observed,
 295 further verifying their intramolecular behaviors for the long-wavelength emission.



296

297 **Fig. 6. Structural analysis of *p*-TBPM, *m*-TBPM, and *o*-TBPM and photoluminescence**
 298 **working mechanism. a** Chemical structures of *p*-TBPM, *m*-TBPM, and *o*-TBPM. **b** Structural
 299 conformation of *p*-TBPM, *m*-TBPM, and *o*-TBPM in the crystalline state. **c-e** Schematic diagram of
 300 potential energy surface and electronic behaviors of (c) *p*-TBPM, (d) *m*-TBPM, and (e) *o*-TBPM.

301 Accordingly, a complete picture of the working mechanism and different CL properties from
 302 these isomers was summarized (Fig. 6c-e). When compounds are excited from the ground state
 303 (S_0) to the excited state (S_1), some excitons release energy through the TBC-based radiative
 304 channel with short-wavelength emission from biphenyl units. Meanwhile, some excitons could

305 relax to the low-energy state caused by the TSC of three isolated biphenyl groups, emitting
306 long-wavelength CL. It is worth noting that the efficiency of CL is mainly determined by the
307 strength of TSC and the stability of the corresponding conformation. The former mainly focuses
308 on the magnitude of electron communication, and the latter is achieved by the rigid molecular
309 skeleton and surrounding environment (e.g., multiple intermolecular interactions). Therefore,
310 structural conformation plays an essential role in manipulating the CL properties of these isomers.
311 (1) For the structurally symmetric *p*-TBPM, the flexibility of its skeleton allows the formation of
312 TSC upon excitation from the ground state to the excited state. However, its flexible skeleton with
313 active molecular motions cannot be totally restricted via multiple intermolecular interactions,
314 resulting in multiple vibrational energy levels. Therefore, *p*-TBPM produces intrinsic emission
315 from biphenyl units and CL from TSC with a moderate FWHM of 53 nm and comparable Φ of
316 55% (**Fig. 6c**). (2) For *m*-TBPM with asymmetric conformation and rigid molecular skeleton,
317 numerous intermolecular interactions can largely stabilize the formed TSC, provide a fixed
318 environment to block molecular motions, and minimize vibrational energy levels.^{59,60} As a result,
319 most excitons can relax to the TSC-based state to produce excitation-independent and narrowband
320 CL with an FWHM of 40 nm and a quantitative Φ of 100% in the crystalline state (**Fig. 6d**). To
321 the best of our knowledge, it is the first time that nonconjugated luminogens have achieved 100%
322 quantum yield, and the FWHM value is comparable to reported conjugated compounds with
323 narrowband emission. It is worth noting that TSC-based narrowband emission can also avoid the
324 wide shoulder peaks in some traditional conjugated luminogens with multiple resonance effect
325 (e.g., perylene), further improving the color purity of luminescence.⁶¹⁻⁶³ (3) For symmetric
326 *o*-TBPM, although the crowded subunits endow it with the largest overlap of electrons to form
327 TSC and the longest wavelength of CL at 390 nm, steric hindrance and weak intermolecular
328 interactions cause the flexible skeleton and dynamic molecular motions to deactivate the formed
329 TSC. Thus, a large portion of energy dissipates via nonradiative decay, and a small part of
330 excitons relaxes via the TSC-based channel with a broad emission peak (FWHM > 70 nm) and a
331 much low Φ of 4% (**Fig. 6e**).

332

333 Discussion

334 Achieving efficient CL via spatial electron interaction and narrowband emission
335 simultaneously seems contradictory. In this work, biphenyl is utilized as a building block to
336 construct a series of nonconjugated luminogens with CL properties. Two molecule-engineering
337 strategies have been utilized to manipulate TSC and CL: (1) Introducing building blocks of
338 biphenyl units enhances the strength of intramolecular TSC, which promotes the shift of
339 luminescence from the TBC-based channel to the TSC-based CL; (2) Constitutionally adjusting
340 the connection positions of building blocks affects structural conformation and intermolecular
341 interactions, which regulate the stability of TSC and efficiency of CL. Different from the
342 structurally symmetric *p*-TBPM and *o*-TBPM with flexible skeleton, *m*-TBPM with asymmetric

343 conformation exhibits multiple intermolecular interactions and rigid skeleton to promote the
344 formation and stabilization of TSC, achieving narrowband CL with an FWHM of 40 nm and
345 100% efficiency. The narrowband emission and luminescent efficiency of this nonconjugated
346 compound are highly competitive to traditional luminogens with extended conjugated and planar
347 structures. This work highlights the critical role of structural conformation in manipulating the
348 photophysical properties of nonconventional luminescent materials and provides a strategy for
349 developing narrowband CL with improved properties.

350

351 **Methods**

352 **Materials.** All chemicals and reagents were purchased from commercial sources such as Bide
353 Pharmatech Ltd., Energy Chemical, Thermo Fisher Scientific, J&K Scientific, and TCI. Common
354 reagents and raw materials were purchased from formal channels, analytically pure, and used without
355 further purification. All the final products used in experiments were purified by silica gel column. The
356 purification of all designed samples was carefully checked by HPLC. Tetrahydrofuran (THF),
357 acetonitrile (ACN), and water used for photophysical measurements were all checked by HPLC.

358 **Instrumentation.** ^1H and ^{13}C nuclear magnetic resonance spectra were recorded on a Bruker
359 AVANCE NEO 600-MHz instrument. UV-vis absorption spectra were recorded by a mid-range UV
360 spectrophotometer (UV-2600i, SHIMADZU). Steady photoluminescence (PL) measurements of all
361 samples were performed on an RF-6000 spectrofluorometer (SHIMADZU) and FLS5
362 Photoluminescence Spectrometer (Edinburgh Instrument). Fluorescence lifetime was measured by
363 FLS1000 Photoluminescence Spectrometer (Edinburgh Instrument). Absolute fluorescence quantum
364 yields were measured on FLS5 Photoluminescence Spectrometer (Edinburgh Instrument) at least three
365 times. Single-crystal X-ray diffraction (XRD) data were collected on a Rigaku Oxford Diffraction
366 SuperNova with Atlas Diffractometer (RIGAKU), and crystal structures were solved with Olex2 (a
367 software, <https://www.olexsys.org/olex2/>). HPLC measurements were carried out on Agilent 1260
368 Infinity II instrument with Agilent 10 (Prep-C18, 250 × 21.2 mm) column, using THF. High-resolution
369 mass spectra of these compounds were all obtained through Fourier transform mass spectrometry
370 (FTMS), and the test instrument is Thermo Scientific Exactive GC Orbitrap (Thermo Scientific).

371 **Computational details.** All the compounds were fully optimized with the density functional theory
372 (DFT) method by using M06-2X density functional and 6-31G(d,p) basis set. London-dispersion
373 effects were also taken into consideration using Grimme's DFT-D3 correction. Analytical frequency
374 calculations were also performed at the same level of theory to confirm that the optimized structures
375 were at a minimum point. Time-dependent density functional theory (TD-DFT) was utilized at the
376 same level of theory to calculate optimized excited (S_1) geometries and energy levels. All the above
377 quantum chemical calculations were carried out using Gaussian 16 program.⁶⁴ Reorganization energy
378 analysis was performed using the Molecular Materials Property Prediction Package (MOMAP).⁶⁵⁻⁶⁷
379 Besides, the Hirshfeld surfaces and decomposed fingerprint plots were calculated and mapped using

380 CrystalExplorer 17.5 package⁶⁸, and the hole-electron analysis were calculated using Multiwfn⁶⁹ and
381 displayed using VMD.⁷⁰

382 **Data availability**

383 The authors declare that all the data supporting the findings of this manuscript are available within
384 the manuscript and Supplementary Information files and available from the corresponding authors
385 upon reasonable request. The X-ray crystallographic coordinates for structures reported in this
386 study have been deposited at the Cambridge Crystallographic Data Centre (CCDC) under
387 deposition numbers of *p*-TBPM (2310837), *m*-TBPM (2310838), *o*-TBPM (2310839). These data
388 can be obtained free of charge from The Cambridge Crystallographic Data Centre via
389 www.ccdc.cam.ac.uk/data_request/cif.

390 **Acknowledgments**

391 This work was supported by the National Natural Science Foundation of China (22205197) and
392 the China Postdoctoral Science Foundation (2022M712721). J.Z. acknowledged the support from
393 the Research Grants Council of the Hong Kong Special Administrative Region, China (HKUST
394 PDFS2324-6S01).

395 **Author contributions**

396 Y.W. and J.Z. performed research, wrote the original draft of the article and carried out theoretical
397 calculation. W.T., L.W., and Y.X. contributed synthesis. J.Z.S. and F.H. participated in the
398 discussion. H.Z. and B.Z.T. contributed to project administration, funding acquisition, and
399 revision of the article.

400 **Competing interests**

401 The authors declare no competing interests.

402 **Reference**

- 403 1. Zhang, X., Li, J., Ma, C., Zhang, H., & Liu, K. Biomimetic Structural Proteins: Modular Assembly and High
404 Mechanical Performance. *Acc. Chem. Res.* **56**, 2664-2675 (2023).
- 405 2. Steinhart, M., Wehrspohn, R.B., Gosele, U., & Wendorff, J.H. Nanotubes by Template Wetting: A Modular
406 Assembly System. *Angew. Chem. Int. Ed.* **43**, 1334-1344 (2004).
- 407 3. Zhang S. Fabrication of novel biomaterials through molecular self-assembly. *Nat. Biotechnol.* **21**, 1171-1178
408 (2003).
- 409 4. Lu, X., & Chen, Z.F. Curved Pi-Conjugation, Aromaticity, and the Related Chemistry of Small Fullerenes
410 (<C60) and Single-Walled Carbon Nanotubes. *Chem. Rev.* **105**, 3643-3696 (2005).
- 411 5. Yan, L., *et al.* Chemistry and Physics of a Single Atomic Layer: Strategies and Challenges for
412 Functionalization of Graphene and Graphene-based Materials. *Chem. Soc. Rev.* **41**, 97-114 (2012).
- 413 6. Bekyarova, E., *et al.* Effect of covalent chemistry on the electronic structure and properties of carbon
414 nanotubes and graphene. *Acc. Chem. Res.* **46**, 65-76 (2013).
- 415 7. Fitzgibbons, T.C., *et al.* Benzene-derived carbon nanothreads. *Nat. Mater.* **14**, 43-47 (2015).

- 416 8. Li, D., Wang, J., & Ma, X. White-Light-Emitting Materials Constructed from Supramolecular Approaches.
417 *Adv. Optical. Mater.* **6**, 1800273 (2018).
- 418 9. Takeda, Y., Data, P., & Minakata, S. Alchemy of Donor–Acceptor–Donor Multi-photofunctional Organic
419 Materials: from Construction of Electron-deficient Azaaromatics to Exploration of Functions. *Chem. Commun.*
420 **56**, 8884-8894 (2020).
- 421 10. Duan, L., Qiao, J., Sun, Y., & Qiu, Y. Strategies to Design Bipolar Small Molecules for OLEDs:
422 Donor-Acceptor Structure and Non-Donor-Acceptor Structure. *Adv. Mater.* **23**, 1137-1144 (2011).
- 423 11. Tang, S., *et al.* Nonconventional luminophores: Characteristics, Advancements and Perspectives. *Chem. Soc.*
424 *Rev.* **50**, 12616–12655 (2021).
- 425 12. Zhang, J., *et al.* Stimuli-Responsive AIEgens. *Adv. Mater.* **33**, 2008071 (2021).
- 426 13. Xu, S., Duan, Y., & Liu, B. Precise Molecular Design for High-Performance Luminogens with
427 Aggregation-Induced Emission. *Adv. Mater.* **32**, 1903530 (2020).
- 428 14. Chen, X., Zhang, X., Xiao, X., Wang, Z., & Zhao, J. Recent Developments on Understanding Charge Transfer
429 in Molecular Electron Donor-Acceptor Systems. *Angew. Chem. Int. Ed.* **62**, e202216010 (2023).
- 430 15. Hong, X., *et al.* TADF molecules with π -extended acceptors for simplified high-efficiency blue and white
431 organic light-emitting diodes. *Chem*, **8**, 1705-1719 (2022).
- 432 16. Yamaguchi, Y., Matsubara, Y., Ochi, T., Wakamiya, T., and Yoshida, Z.I. How the π Conjugation Length
433 Affects the Fluorescence Emission Efficiency. *J. Am. Chem. Soc.* **130**, 13867-13869 (2008).
- 434 17. Yang, J., *et al.* Constitutional isomerism of the linkages in donor–acceptor covalent organic frameworks and
435 its impact on photocatalysis. *Nat. Commun.* **13**, 6317 (2022).
- 436 18. Zhang, H., & Tang B.Z. Through-Space Interactions in Clusteroluminescence. *JACS Au* **1**, 1805–1814 (2021).
- 437 19. Sakhno, T.V., Sakhno, Y.E., & Kuchmiy, S.Y. Clusteroluminescence of Unconjugated Polymers: A Review.
438 *Theor. Exp. Chem.* **59**, 75-106 (2023).
- 439 20. Zheng, S., Zhu, T., Wang, Y., Yang, T., & Yuan, W.Z. Accessing Tunable Afterglows from Highly Twisted
440 Nonaromatic Organic AIEgens via Effective Through-Space Conjugation. *Angew. Chem. Int. Ed.* **59**, 10018–
441 10022 (2020).
- 442 21. Li, Q., *et al.* Through-Space Charge-Transfer Polynorbornenes with Fixed and Controllable Spatial Alignment
443 of Donor and Acceptor for High-Efficiency Blue Thermally Activated Delayed Fluorescence. *Angew. Chem.*
444 *Int. Ed.* **59**, 20174–20182 (2020).
- 445 22. Zhang, H., *et al.* Why Do Simple Molecules with "Isolated" Phenyl Rings Emit Visible Light? *J. Am. Chem.*
446 *Soc.* **139**, 16264-16272 (2017).
- 447 23. Chu, B., *et al.* Aliphatic Polyesters with White-Light Clusteroluminescence. *J. Am. Chem. Soc.* **144**,
448 15286-15294 (2022).

- 449 24. He, B., *et al.* Clusteroluminescence from Cluster Excitons in Small Heterocyclics Free of Aromatic Rings. *Adv.*
450 *Sci.* **8**, 2004299 (2021).
- 451 25. Li, H., *et al.* As Fiber Meets with AIE: Opening a Wonderland for Smart Flexible Materials. *Adv. Mater.* **35**,
452 2210085 (2023).
- 453 26. Kong, D., Zhang, K., Tian, J., Yin, L., & Sheng, X. Biocompatible and Biodegradable Light-Emitting
454 Materials and Devices. *Adv. Mater. Technol.* **7**, 2100006 (2022).
- 455 27. Liu, J., *et al.* Through-Space Interaction of Tetraphenylethylene: What, Where, and How. *J. Am. Chem. Soc.*
456 **144**, 7901-7910 (2022).
- 457 28. Feig, V.R., Tran, H., & Bao, Z. Biodegradable Polymeric Materials in Degradable Electronic Devices. *ACS*
458 *Cent. Sci.* **4**, 337-348 (2018).
- 459 29. Zhao, D., *et al.* Cellulose-Based Flexible Functional Materials for Emerging Intelligent Electronics. *Adv.*
460 *Mater.* **33**, 2000619 (2021).
- 461 30. Ying, L., Ho, C.L., Wu, H., Cao, Y., & Wong, W.Y. White Polymer Light-Emitting Devices for Solid-State
462 Lighting: Materials, Devices, and Recent Progress. *Adv. Mater.* **26**, 2459–2473 (2014).
- 463 31. Zhang, Z., *et al.* Manipulation of Clusteroluminescence in Carbonyl-based Aliphatic Polymers. *Aggregate* **3**,
464 e278 (2022).
- 465 32. Zhang, J., *et al.* How to Manipulate Through-Space Conjugation and Clusteroluminescence of Simple AIEgens
466 with Isolated Phenyl Rings. *J. Am. Chem. Soc.* **143**, 9565-9574 (2021).
- 467 33. Zhang, H., *et al.* Clusterization-triggered Emission: Uncommon Luminescence from Common Materials.
468 *Mater. Today* **32**, 275-292 (2020).
- 469 34. Li, J., Shen, P., Zhao, Z., & Tang, B.Z. Through-Space Conjugation: A Thriving Alternative for
470 Optoelectronic Materials. *CCS Chem.* **1**, 181-196 (2019).
- 471 35. Liao, P., *et al.* Generating Circularly Polarized Luminescence from Clusterization-triggered Emission Using
472 Solid Phase Molecular Self-Assembly. *Nat. Commun.* **12**, 5496 (2021).
- 473 36. Li, Q., *et al.* Pillararene-Induced Intramolecular Through-Space Charge Transfer and Single-Molecule
474 White-Light Emission. *Angew. Chem. Int. Ed.* **61**, e202202381 (2022).
- 475 37. Viglianti, L., *et al.* Unusual Through-Space Interactions between Oxygen Atoms that Mediate Inverse
476 Morphochromism of an AIE Luminogen. *Angew. Chem. Int. Ed.* **59**, 8552–8559 (2020).
- 477 38. Li, Q., *et al.* Molecular-level enhanced clusterization-triggered emission of nonconventional luminophores in
478 dilute aqueous solution. *Nat. Comm.* **14**, 409 (2023).
- 479 39. Chu, B., *et al.* Altering Chain Flexibility of Aliphatic Polyesters for Yellow-Green Clusteroluminescence in
480 38 % Quantum Yield. *Angew. Chem. Int. Ed.* **61**, e202114117 (2022).

- 481 40. Zhang, J., *et al.* Secondary Through-space Interactions Facilitated Single-molecule White-light Emission from
482 Clusteroluminogens. *Nat. Commun.* **13**, 3492 (2022).
- 483 41. Zhang, Z., *et al.* NIR Clusteroluminescence of Non-conjugated Phenolic Resins Enabled by Through-Space
484 Interactions. *Angew. Chem. Int. Ed.* **62**, e202306762 (2023).
- 485 42. Kim, Y.H., Cho, H., & Lee, T.W. Metal halide perovskite light emitters. *Proc. Natl. Acad. Sci. USA* **113**,
486 11694–11702 (2016).
- 487 43. Zhao, Z., Zhang, H., Lam, J.W.Y., & Tang, B.Z. Aggregation-Induced Emission: New Vistas at the Aggregate
488 Level. *Angew. Chem. Int. Ed.* **59**, 9888-9907 (2020).
- 489 44. Naveen, K.R., Oh, J.H., Lee, H.S., & Kwon, J.H. Tailoring Extremely Narrow FWHM in Hypsochromic and
490 Bathochromic Shift of Polycyclo-Heteraborin MR-TADF Materials for High-Performance OLEDs. *Angew.*
491 *Chem. Int. Ed.* **62**, e202306768 (2023).
- 492 45. Qu, Y.K., *et al.* Steric Modulation of Spiro Structure for Highly Efficient Multiple Resonance Emitters. *Angew.*
493 *Chem. Int. Ed.* **61**, e202201886 (2022).
- 494 46. Liu, J., *et al.* Toward a BT.2020 green emitter through a combined multiple resonance effect and multi-lock
495 strategy. *Nat. Commun.* **13**, 4876 (2022).
- 496 47. Song, B., *et al.* Facile Conversion of Water to Functional Molecules and Cross-linked Polymeric Films with
497 Efficient Clusteroluminescence. *Nat. Commun.* **14**, 3115 (2023).
- 498 48. Zhang, J., *et al.* White-light Emission from Organic Aggregates: a Review. *Adv. Photonics.* **4**, 014001 (2021).
- 499 49. Shi, C.Y., *et al.* Dynamic Supramolecular H-bonding Network with Orthogonally Tunable
500 Clusteroluminescence. *Angew. Chem. Int. Ed.* **62**, e202214422 (2023).
- 501 50. Xiong, Z., Zhang, J., Sun, J.Z., Zhang, H., & Tang, B.Z. (2023). Excited-State Odd–Even Effect in
502 Through-Space Interactions. *J. Am. Chem. Soc.* **145**, 21104-21113.
- 503 51. Qiu, W., *et al.* Afterglow OLEDs Incorporating Bright Closely Stacked Molecular Dimers with Ultra-long
504 Thermally Activated Delayed Fluorescence. *Matter* **6**, 1231-1248 (2023).
- 505 52. Madayanad Suresh, S., Hall, D., Beljonne, D., Olivier, Y., & Zysman-Colman, E. Multiresonant Thermally
506 Activated Delayed Fluorescence Emitters Based on Heteroatom-Doped Nanographenes: Recent Advances and
507 Prospects for Organic Light-Emitting Diodes. *Adv. Funct. Mater.* **30**, 1908677 (2020).
- 508 53. Han, J., *et al.* Narrowband Blue Emission with Insensitivity to the Doping Concentration from An
509 Oxygen-bridged Triarylboron-based TADF Emitter: Nondoped OLEDs with A High External Quantum
510 Efficiency up to 21.4%. *Chem. Sci.* **13**, 3402-3408 (2022).
- 511 54. Yang, W., *et al.* An Effective Approach toward Yellow-to-Orange Multi-Resonance TADF Emitters by
512 Integrating Strong Electron Donor into B/N-Based Polycyclic Architecture: High Performance OLEDs with
513 Nearly 40% EQE. *Adv. Funct. Mater.* **33**, 2213056 (2023).

- 514 55. Luo, S., *et al.* Regulation of Multiple Resonance Delayed Fluorescence via Through-Space Charge Transfer
515 Excited State towards High-Efficiency and Stable Narrowband Electroluminescence. *Angew. Chem. Int. Ed.* **62**,
516 e202310943 (2023).
- 517 56. Spackman, M.A., & Jayatilaka, D. Hirshfeld Surface Analysis. *CrystEngComm* **11**, 19-32 (2009).
- 518 57. Zhang, H., *et al.* Drawing a Clear Mechanistic Picture for the Aggregation-Induced Emission Process. *Mater.*
519 *Chem. Front.* **3**, 1143-1150 (2019).
- 520 58. Shuai, Z., & Peng, Q. Organic Light-Emitting Diodes: Theoretical Understanding of Highly Efficient Materials
521 and Development of Computational Methodology. *Natl. Sci. Rev.* **4**, 224-239 (2017).
- 522 59. Tu, W., *et al.* Manipulation of the Through-space Interactions in Diphenylmethane, *Smart Molecules*, **1**,
523 e20220006 (2023).
- 524 60. Liu, F.M., *et al.* Toward narrowband emission: the chemical strategies for modifying boron-based luminescent
525 materials. *J. Mater. Chem. C* **11**, 11425-11439 (2023).
- 526 61. Kondo, Y., *et al.* Narrowband Deep-blue Organic Light-Emitting Diode Featuring an Organoboron-based
527 Emitter. *Nat. Photonics* **13**, 678-682 (2019).
- 528 62. Naveen, K.R., Hwang, S.J., Lee, H., & Kwon, J.H. Narrow Band Red Emission Fluorophore with Reasonable
529 Multiple Resonance Effect. *Adv. Electron. Mater.* **8**, 2101114 (2022).
- 530 63. Liao, X.J., *et al.* Planar Chiral Multiple Resonance Thermally Activated Delayed Fluorescence Materials for
531 Efficient Circularly Polarized Electroluminescence. *Angew. Chem. Int. Ed.* **62**, e202217045 (2023).
- 532 64. Frisch, M.J., *et al.* Gaussian 16, Gaussian, Inc., Wallingford CT (2016).
- 533 65. Shuai, Z. Thermal Vibration Correlation Function Formalism for Molecular Excited State Decay Rates. *Chin. J.*
534 *Chem.* **38**, 1223-1232 (2020).
- 535 66. Shuai, Z., & Peng, Q. Excited States Structure and Processes: Understanding Organic Light-emitting Diodes at
536 the Molecular Level. *Phys. Rep.* **537**, 123-156 (2014).
- 537 67. Shuai, Z., & Peng, Q. Organic Light-emitting Diodes: Theoretical Understanding of Highly Efficient Materials
538 and Development of Computational Methodology. *Natl. Sci. Rev.* **4**, 224-239 (2017).
- 539 68. Spackman, M.A., & Jayatilaka, D. Hirshfeld Surface Analysis. *CrystEngComm* **11**, 19-32 (2009).
- 540 69. Lu, T., & Chen, F. Multiwfn: A multifunctional wavefunction analyzer. *J. Comput. Chem.* **33**, 580-592 (2012).
- 541 70. Humphrey, W., Dalke, A., & Schulten, K.. VMD-Visual Molecular Dynamics. *J. Molec. Graphics* **14**, 33-38
542 (1996).